

Live-Cell RNA Imaging with Metabolically Incorporated Fluorescent Nucleosides

Danyang Wang, Ana Shalamberidze, A. Emilia Arguello, Byron W. Purse,* and Ralph E. Kleiner*



Cite This: *J. Am. Chem. Soc.* 2022, 144, 14647–14656



Read Online

ACCESS |



Metrics & More

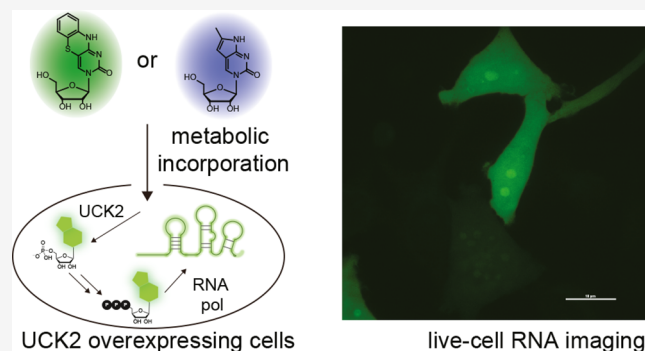


Article Recommendations



Supporting Information

ABSTRACT: Fluorescence imaging is a powerful method for probing macromolecular dynamics in biological systems; however, approaches for cellular RNA imaging are limited to the investigation of individual RNA constructs or bulk RNA labeling methods compatible primarily with fixed samples. Here, we develop a platform for fluorescence imaging of bulk RNA dynamics in living cells. We show that fluorescent bicyclic and tricyclic cytidine analogues can be metabolically incorporated into cellular RNA by overexpression of uridine–cytidine kinase 2. In particular, metabolic feeding with the tricyclic cytidine-derived nucleoside tC combined with confocal imaging enables the investigation of RNA synthesis, degradation, and trafficking at single-cell resolution. We apply our imaging modality to study RNA metabolism and localization during the oxidative stress response and find that bulk RNA turnover is greatly accelerated upon NaAsO₂ treatment. Furthermore, we identify cytoplasmic RNA granules containing RNA transcripts generated during oxidative stress that are distinct from canonical stress granules and P-bodies and co-localize with the RNA helicase DDX6. Taken together, our work provides a powerful approach for live-cell RNA imaging and reveals how cells reshape RNA transcriptome dynamics in response to oxidative stress.



INTRODUCTION

RNA plays a central role in biology, and probing its dynamic behavior is critical for illuminating the mechanisms underlying fundamental biological processes. A powerful approach to study the lifecycle of cellular RNA, including its transcription, trafficking, and decay, is fluorescence microscopy.¹ Current approaches for visualizing RNA dynamics in living cells have primarily focused on imaging individual transcripts. This can be accomplished in several ways. Singer and co-workers developed MS2 tagging,² which uses a viral MS2 stem-loop sequence to recruit a green fluorescent protein (GFP)-fusion protein to the RNA of interest and has been the gold standard for live-cell RNA imaging over the last three decades. More recently, fluorescent RNA aptamers³ and CRISPR-Cas targeting strategies⁴ have provided complementary methods to image individual RNA sequences in cells. Furthermore, RNAs generated in vitro or purified from cells can be chemoenzymatically modified with synthetic fluorophores and then introduced into cells.⁵ These methods for live-cell RNA imaging have provided important biological insights but are restricted to analyzing individual transcripts and typically require the addition of non-native RNA sequence tags.

A complementary approach for the investigation of cellular RNA dynamics is the incorporation of modified nucleosides into cellular RNA.⁶ We and others have reported that modified pyrimidine and purine nucleosides containing alkyne,⁷

azide,^{8–10} or vinyl¹¹ functionality can be incorporated into RNA through nucleotide salvage pathways, labeled with fluorescent dyes using bio-orthogonal chemistry, and used to visualize RNA in intact cells and organisms. Depending in part upon the ribonucleoside structure, the power of metabolic labeling lies in its simplicity and transcriptome-wide generality. Azide/alkyne-modifications that minimally perturb nucleoside structure can be accepted by nucleotide salvage pathways and incorporated into RNA in living cells; however, imaging of these metabolically incorporated bio-orthogonal ribonucleosides has been performed largely in fixed cells or tissue sections. This is primarily due to reliance on Cu(I)-catalyzed azide–alkyne cycloaddition (CuAAC)¹² for fluorescent labeling, which is incompatible with living cells as well as the need to “wash out” excess unreacted dye used to drive the labeling reaction to completion. While these approaches are powerful, bio-orthogonal labeling protocols can introduce bias due to fixation and permeabilization methods, or as a result of non-

Received: April 21, 2022

Published: August 5, 2022



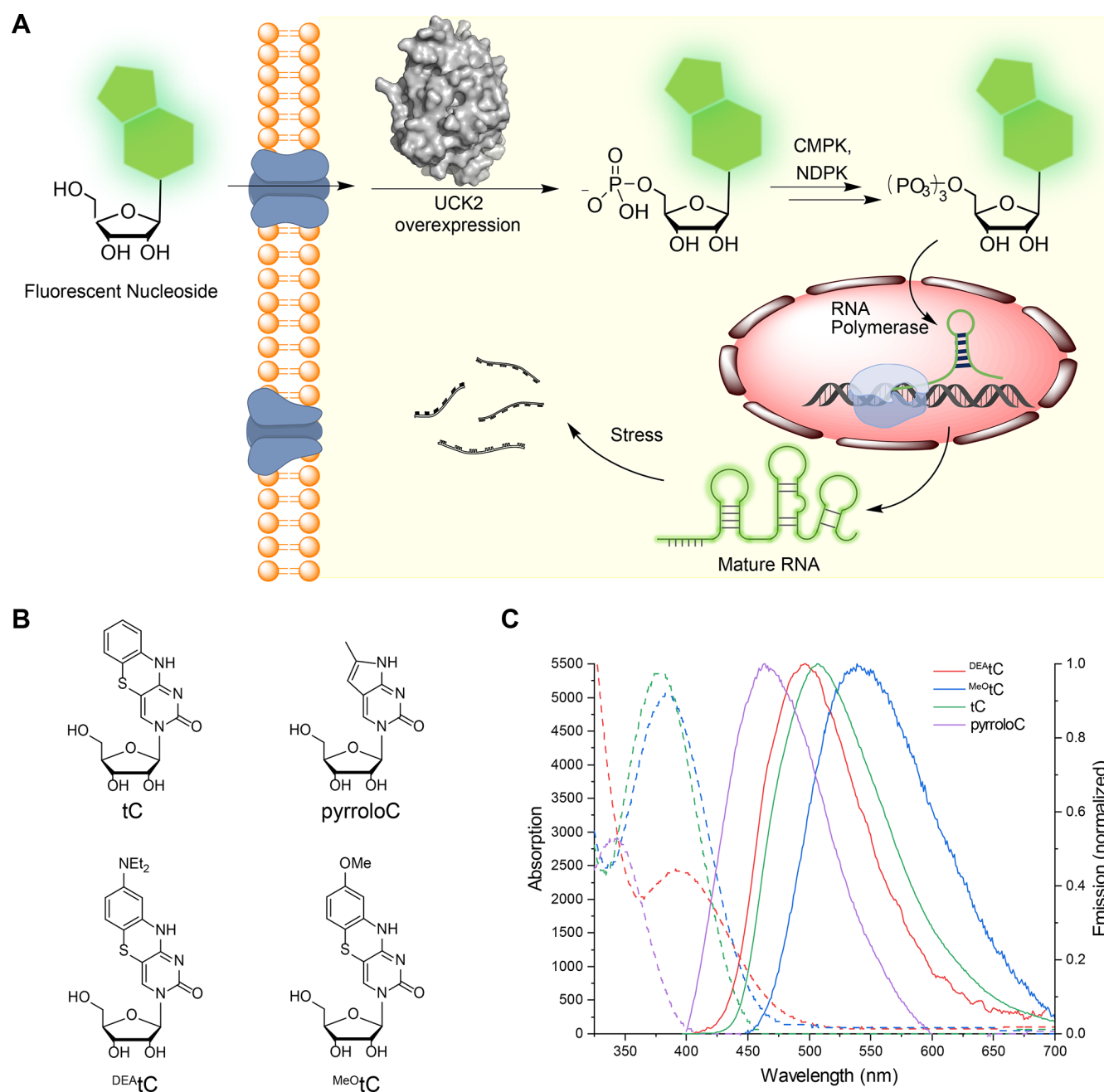


Figure 1. Metabolic incorporation of fluorescent nucleosides into cellular RNAs. (A) Scheme for incorporation of fluorescent nucleosides through the nucleotide salvage pathway. (B) Structure of fluorescent nucleosides used in this work. (C) Absorption (dashed) and corrected emission (solid) spectra of fluorescent ribonucleoside analogues used in this study. Spectra were recorded at 295 K in 1× PBS buffer, pH 7.4.

specific binding of the fluorescent dye to cellular structures, and therefore, it is unknown whether these methods accurately capture a snapshot of all cellular RNAs. In a few instances, strain-promoted azide–alkyne cycloaddition (SPAAC) chemistry has been utilized to label azido-modified RNA with fluorescent dyes in living cells;^{9,10} however, the slow kinetics of this reaction, requirement for cell permeable fluorescent dyes, and difficulty in removing excess fluorophore make its application challenging to intracellular targets.

An alternative to the two-step procedure used for imaging RNA with bio-orthogonal ribonucleosides would be the direct metabolic incorporation of a fluorescent nucleoside (Figure 1a). Since this strategy would not require a fluorophore labeling reaction after RNA incorporation and the fluorescence

of an RNA transcript containing multiple modified nucleosides should exceed the fluorescence background from individual modified nucleosides or nucleotides, it should enable live-cell RNA imaging of global transcriptome dynamics. Indeed, a large number of fluorescent nucleoside analogues have been reported;¹³ however, these structures have been primarily used for *in vitro* applications and incorporated into RNA using chemical synthesis or *in vitro* transcription, and it is unknown whether they are suitable substrates for metabolic incorporation into RNA.

Previously, we showed that phosphorylation by uridine–cytidine kinase 2 (UCK2) is the bottleneck for the metabolic incorporation of C5-modified pyrimidine nucleosides and that expression of a mutant form of the kinase enabled metabolic

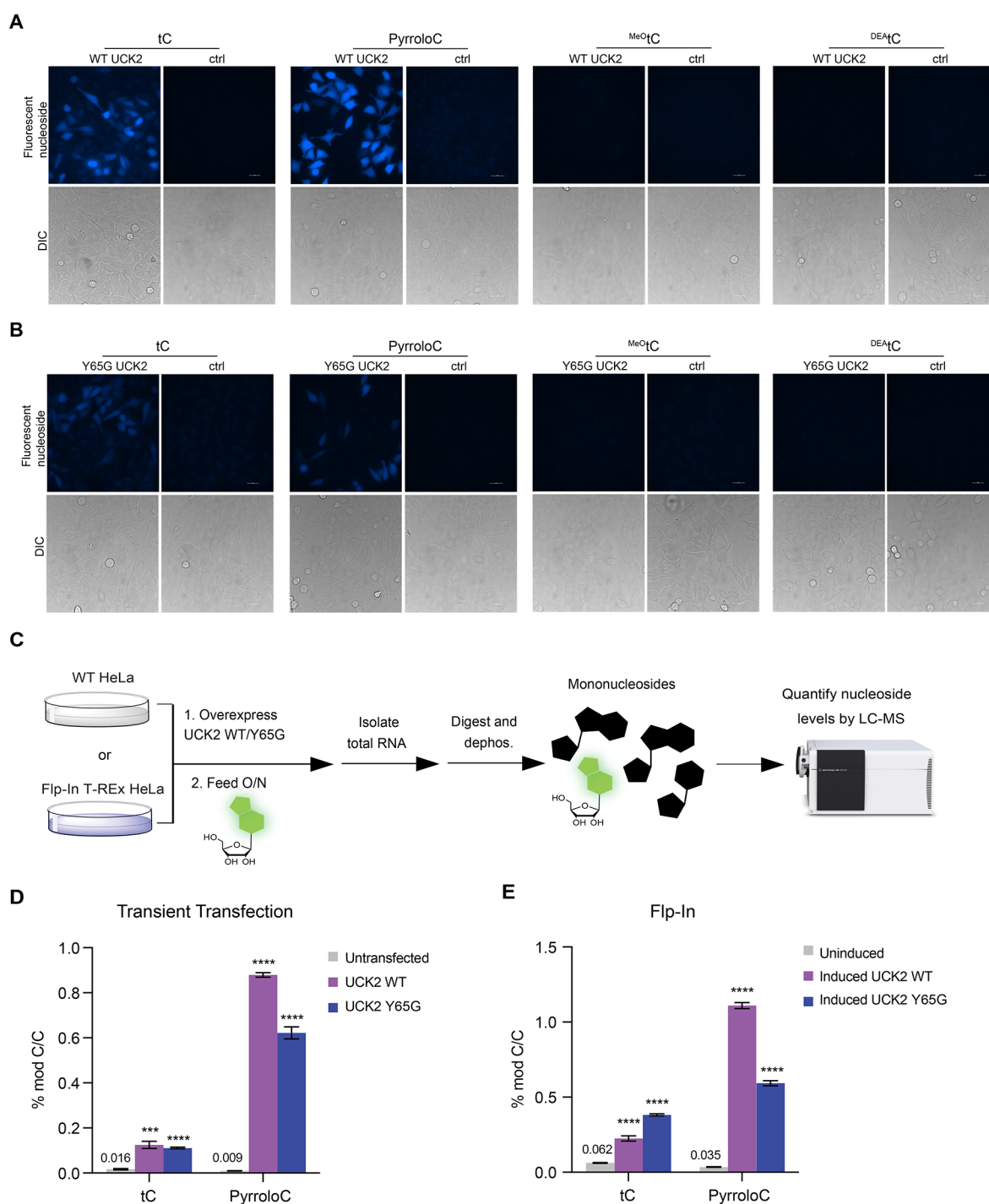


Figure 2. Detection of fluorescent nucleoside incorporation into cellular RNA using imaging and LC-MS. (A) Incorporation of fluorescent nucleosides into HeLa Flp-In WT UCK2 cells. UCK2 expression was induced with tetracycline, and cells were treated with 500 μ M nucleoside for 12 h and imaged. Tetracycline induction was omitted to serve as a control for UCK2 expression. (B) Incorporation of fluorescent nucleosides into HeLa Flp-In Y65G UCK2 cells. Cells were treated and imaged as in (A). (C) Workflow for quantitation of fluorescent nucleosides in cellular RNA using LC-MS. (D) RNA incorporation of tC or pyrroloC into HeLa cells transfected with UCK2 constructs. (E) RNA incorporation of tC or pyrroloC in HeLa cell lines stably expressing inducible UCK2 WT or Y65G mutants.

labeling with 5-azidomethyluridine (5-AmU).⁹ Herein, we evaluate the *in vitro* phosphorylation and RNA metabolic incorporation of a series of fluorescent cytidine analogues. We demonstrate that expression of UCK2 in cells facilitates RNA labeling with pyrrolocytidine (pyrroloC)¹⁴ and 1,3-diaza-2-oxophenothiazine (tC)¹⁵ fluorescent ribonucleosides. Furthermore, we use the UCK2 system combined with tC feeding and

confocal microscopy in order to measure RNA transcription, turnover, and trafficking in live cells during normal and stress conditions. We reveal the effects of oxidative stress on RNA metabolism and identify the formation of a novel stress-dependent RNA-protein granule. Taken together, our work provides a general approach for live-cell RNA imaging and

reveals the spatiotemporal dynamics of cellular RNA during the oxidative stress response.

RESULTS

Fluorescent Nucleosides for RNA Imaging. In order to label cellular RNA for biological imaging, we selected and evaluated a set of fluorescent pyrimidine nucleosides. Our criteria included commercial availability or synthetic accessibility of the structure, ability of the modified nucleoside to engage in canonical Watson–Crick base pairing, likelihood of compatibility with pyrimidine salvage pathways, and fluorophore brightness and spectral overlap with commonly used imaging modalities in fluorescence microscopy. Therefore, we chose four modestly sized bicyclic and tricyclic fluorescent cytidine analogues containing extended ring systems projecting from the non-Watson Crick face of the molecule (Figure 1b). We measured the absorption and emission spectra and determined the fluorescence quantum yield (Φ_{em}) of these analogues under identical conditions—dilute solutions in 1× PBS buffer (pH 7.4) at 22 °C (Figure 1c, Supporting Information Table 1). PyrroloC^{14,16} is a commercially available bicyclic cytidine analogue for which we measured $\epsilon_{357\text{ nm}} = 2900\text{ M}^{-1}\text{ cm}^{-1}$ and $\Phi_{\text{em},465\text{ nm}} = 0.08$. It has the smallest structural deviation from natural pyrimidine nucleosides among this set and is only modestly quenched by base pairing and stacking, with reported $\Phi_{\text{em},460\text{ nm}} = 0.06$ in duplex DNA or RNA.¹⁷ The remaining three compounds are members of the tC family.¹⁵ The tC ribonucleoside was synthesized following published procedures,¹⁸ and we developed analogous methods to synthesize MeO^tC and DEAtC ribonucleosides, which are reported here (compound synthesis and characterization data are available in the Supporting Information). Parent tC offers robust fluorescence as a free nucleoside with $\epsilon_{377\text{ nm}} = 5400\text{ M}^{-1}\text{ cm}^{-1}$ and $\Phi_{\text{em},513\text{ nm}} = 0.17$ and similar brightness in matched duplex DNA, $\Phi_{\text{em},513\text{ nm}} = 0.11$.^{15,19} DEAtC has little fluorescence as a free nucleoside ($\Phi_{\text{em},493\text{ nm}} = 0.006$) but much higher quantum yield up to $\Phi_{\text{em},500\text{ nm}} = 0.12$ in dsDNA or greater in a DNA–RNA heteroduplex (up to $\Phi_{\text{em}} = 0.20$; unpublished).^{20,21} MeO^tC exhibits intermediate properties, modestly brighter than DEAtC as a free nucleoside ($\Phi_{\text{em},550\text{ nm}} = 0.015$) but with less fluorescence increase upon matched base pairing and stacking in dsDNA ($\Phi_{\text{em},532\text{ nm}} \approx 0.03$).²⁰ The insensitivity of parent tC fluorescence to the local environment is attractive, while DEAtC fluorescence turn-on upon incorporation into a duplex offers potential utility for probing nucleic acid structures in cells.

Metabolic Labeling with Fluorescent Cytidine Analogues. We next evaluated whether the fluorescent nucleosides could be incorporated into living cells. For this purpose, we used HeLa cells stably expressing ribonucleoside kinase UCK2 under the control of a tetracycline-inducible promoter (i.e., Flp-In T-Rex system)⁹ or made to constitutively express UCK2 through transient transfection of a suitable DNA plasmid construct and monitored incorporation using fluorescence microscopy and quantitative nucleoside LC–QQQ–MS. These UCK2 expression systems provide 7–11-fold overexpression above endogenous kinase levels (Supporting Information Figure 1) and the flexibility to utilize mutant kinases,⁹ which we reasoned could be applied to facilitate the phosphorylation and incorporation of fluorescent nucleosides that are incompatible with native nucleotide metabolism.

To test the nucleoside incorporation, we treated cells with each fluorescent nucleoside for 12 h and then imaged cells by

epifluorescence microscopy after removing free nucleoside. PyrroloC, tC, and MeO^tC were used at 500 μM ; DEAtC was used at 200 μM due to cytotoxicity. We chose a DAPI filter set (excitation: $360 \pm 20\text{ nm}$, emission: $460 \pm 25\text{ nm}$) due to its availability on most widefield fluorescence microscopes and since the excitation and emission band pass wavelengths overlapped with the spectra of each of the synthetic nucleosides. Since we could not detect fluorescence in native HeLa cells after feeding (Supporting Information Figure 2), we tested whether induction of UCK2 expression (WT or Y65G mutant) in the HeLa T-Rex Flp-In UCK2 cells could facilitate nucleoside incorporation. Gratifyingly, in cells treated with tC or pyrroloC and induced to express WT or Y65G UCK2, we observed strong fluorescence labeling (Figure 2a,b). The fluorescence signal was concentrated in the nucleus but was also found in the cytoplasm, consistent with RNA incorporation. Interestingly, for both pyrroloC and tC, we observed higher fluorescence in cells overexpressing WT UCK2 as compared to the Y65G mutant, in contrast to our previous results with C5-modified uridine analogues containing acyclic substitutions. In cells without UCK2 overexpression, we detected minimal fluorescence (52-fold less) (Figure 2a,b), indicating that endogenous UCK2 levels are insufficient for robust phosphorylation and incorporation. For MeO^tC and DEAtC derivatives, we were not able to observe fluorescent cellular labeling under any of the conditions tested. In addition, DEAtC displayed significant cytotoxicity after extended treatment time.

To prove that cellular fluorescence is a result of RNA incorporation of pyrroloC and tC, rather than simply nucleoside uptake and phosphorylation, we employed two complementary assays. First, we performed feeding in the presence of actinomycin D (ActD), a potent inhibitor of RNA polymerase I and II. Under these conditions, cellular fluorescence was greatly reduced (15-fold less) (Supporting Information Figure 3). In contrast, co-treatment with hydroxyurea (a DNA synthesis inhibitor) had little effect on labeling. We also performed imaging of pyrroloC- or tC-treated cells after paraformaldehyde fixation and extensive washing (to eliminate fluorescence from free modified nucleotides) and found only a minimal decrease in signal intensity, further supporting that the majority of the observed signal originates from labeled RNA (Supporting Information Figure 4). Second, we isolated total cellular RNA from induced HeLa T-Rex Flp-In UCK2 cells or cells transiently transfected with UCK2 and performed nucleoside LC–QQQ–MS after digestion and dephosphorylation to nucleosides (Figure 2c and Supporting Information Table 2). Strikingly, our results show that overexpression of WT or Y65G UCK2 kinase in either expression system leads to ~20 to 100-fold increase in RNA incorporation of pyrroloC (Figure 2d,e, Supporting Information Tables 3 and 4). The highest level of pyrroloC labeling ($1.1 \pm 0.02\%$ of C) was achieved using cells, stably expressing inducible WT UCK2 (Figure 2e). Similarly, we observed a ~4 to 8-fold increase in RNA labeling with tC upon expression of WT UCK2 or Y65G UCK2, although the overall levels of incorporation were slightly lower than those achieved with pyrroloC nucleoside (Figure 2d,e). We also measured incorporation of DEAtC and MeO^tC using our LC–QQQ–MS assay. We were unable to detect DEAtC nucleoside in digested total RNA (Supporting Information Figure 5, Supporting Information Figure 6, and Supporting Information Table 5), consistent with our cellular imaging experiments (Figure 2a,b).

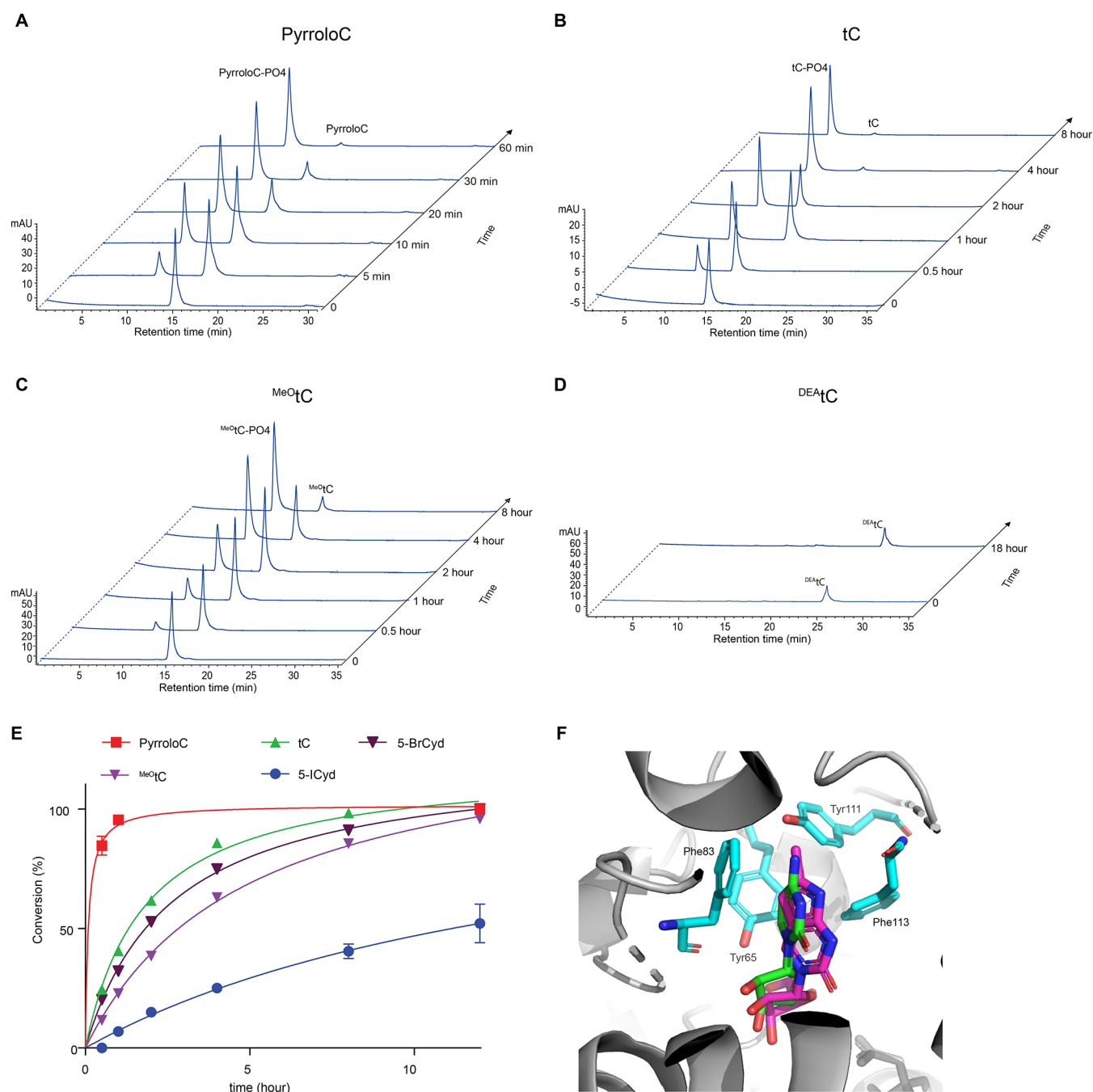


Figure 3. Phosphorylation of fluorescent nucleosides and cytidine analogues by recombinant UCK2. (A–D) HPLC chromatogram time course of pyrroloC (A), tC (B), $^{\text{MeO}}\text{tC}$ (C), and $^{\text{DEA}}\text{tC}$ (D) phosphorylation by recombinant UCK2 WT. (E) Quantification and kinetic analysis of fluorescent nucleoside phosphorylation reactions. Data represent mean \pm SD ($n = 3$). (F) Overlay of simulated pyrroloC (purple) and cytidine (green) bound to UCK2 (PDB: 1UEJ).

While we could measure $0.026 \pm 0.0009\%$ incorporation of $^{\text{MeO}}\text{tC}$ upon UCK2 induction (Supporting Information Figure 6 and Supporting Information Table 5), this level is ~ 10 to 40-fold lower than that with pyrrolo C or tC and likely insufficient to produce robust fluorescence in cells. For tC, we also measured incorporation into small RNA and mRNA in order to prove transcriptome-wide generality of labeling. We found that poly(A)-enriched RNA showed an ~ 2.5 -fold higher tC incorporation rate than total RNA, consistent with mRNA incorporation and rapid mRNA metabolism (Supporting Information Figure 8a,b); tC levels in small RNA were comparable to total RNA. Finally, we also demonstrated tC

incorporation into U2OS cells using transient transfection of UCK2 and epifluorescence microscopy (Supporting Information Figure 9). Taken together, our data demonstrate that efficient metabolic RNA labeling with fluorescent nucleosides pyrrolo C and tC can be achieved through overexpression of nucleoside kinase UCK2. This system should be suitable for live-cell imaging of the bulk RNA population in diverse cell types.

In Vitro Phosphorylation with UCK2. To further understand the incorporation of bulky fluorescent nucleosides into cellular RNA and the involvement of UCK2 in this process, we directly studied the phosphorylation of modified

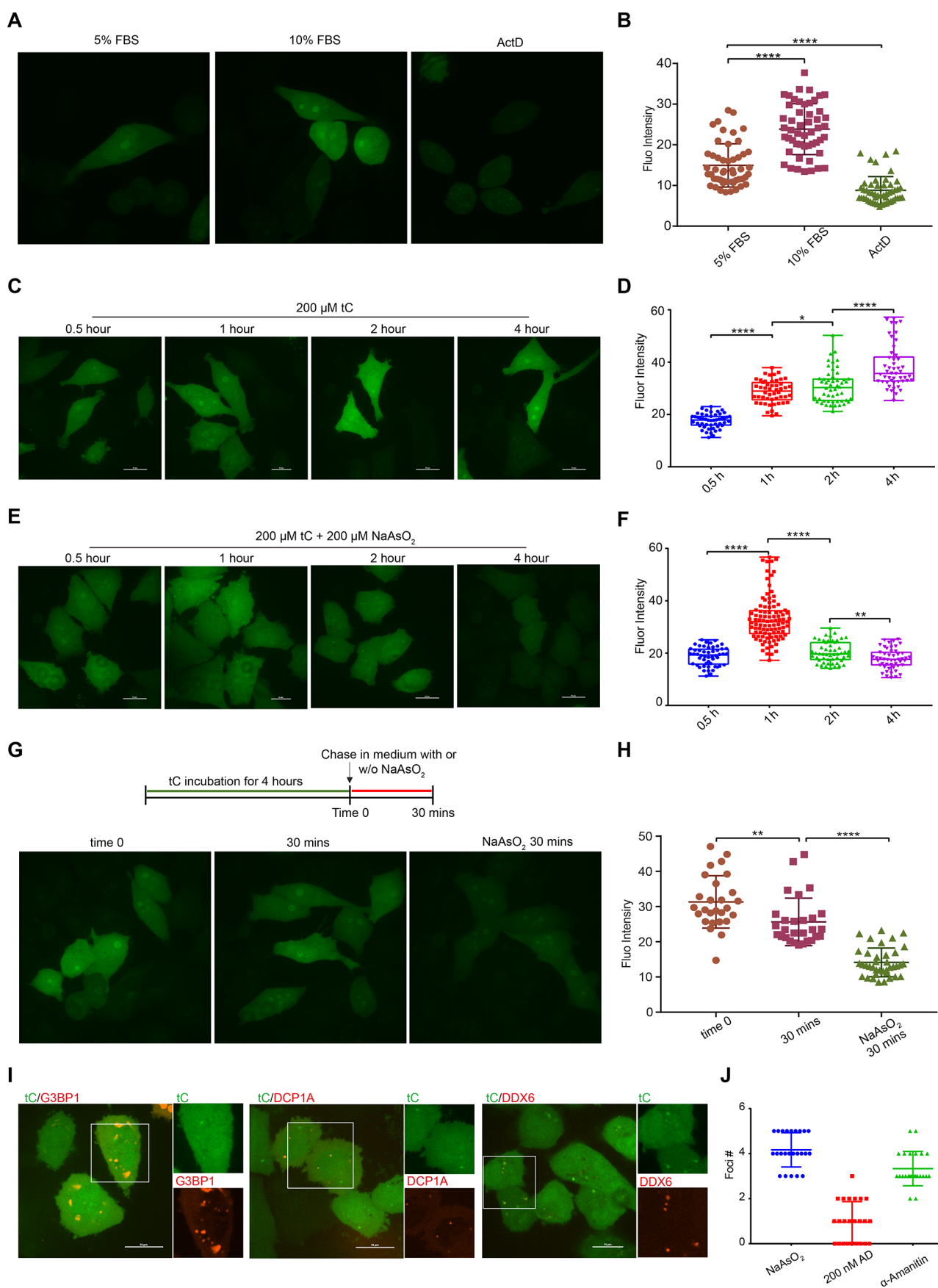


Figure 4. Live-cell imaging of cellular RNA dynamics using tC RNA labeling. (A) Representative images of tC incorporation into cells grown in 5 or 10% FBS or in the presence of ActD. (B) Fluorescence intensity quantification of cells treated in (A). Error bars represent mean \pm s.d. ($n = 50$ cells from three independent biological replicates). (C) Time-course analysis of tC incorporation into cellular RNA. (D) Fluorescence intensity

Figure 4. continued

quantification of cells treated in (C). Error bars represent mean \pm s.d. ($n = 50$ cells from three independent biological replicates). (E) Time-course analysis of tC incorporation into cellular RNA during co-treatment with 200 μ M NaAsO₂. (F) Fluorescence intensity quantification of cells treated in (E). Error bars represent mean \pm s.d. ($n = 50$ cells from three independent biological replicates). (G) Representative images of cells pulsed with tC for 4 h and chased with complete medium or with 200 μ M NaAsO₂ in medium. (H) Fluorescence quantification of cells treated in (G). Error bars represent mean \pm s.d. ($n = 25$ cells from three independent biological replicates). (I) Colocalization of RNA foci formed under stress conditions with G3BP1, DCP1A, or DDX6. (J) Quantification of cellular RNA foci number under stress and RNA synthesis inhibitor treatments. Error bars represent mean \pm s.d. ($n = 25$ cells from three independent biological replicates) (** $P < 0.01$ and **** $P < 0.0001$).

nucleosides by recombinant, purified UCK2 using an HPLC-based *in vitro* assay. As we observed similar RNA incorporation levels in cells expressing either WT or Y65G UCK2, we focused on WT UCK2 since its heterologous expression and purification is more straightforward. Consistent with high-level cellular incorporation, we observed complete phosphorylation of pyrroloC and 42% phosphorylation of tC by UCK2 in 1 h under the conditions assayed (Figure 3a,b and Supporting Information Table 6). Under identical reaction conditions, uridine was completely converted to cytidine monophosphate in 5 min (Supporting Information Figure 10). Similarly, cytidine analogues that were poorly incorporated showed minimal *in vitro* phosphorylation—we detected no phosphorylation of ^{DEA}tC (even after extended reaction times) and only minimal phosphorylation (<20%) of ^{MeO}tC after 1 h (Figure 3c,d and Supporting Information Table 6). Our results show that the incorporation efficiency of bicyclic and tricyclic fluorescent cytidine analogues into cellular RNA correlates strongly with their ability to be phosphorylated by UCK2. Nevertheless, we cannot exclude that other factors including, but not limited to, nucleoside uptake, downstream metabolism, and toxicity of these nucleosides and related metabolites are also strong determinants for metabolic incorporation into cellular RNA.

In our previous work,⁹ we found that modest substitutions at the C5 position severely compromised the ability of uridine nucleosides to serve as substrates for UCK2, likely due to steric clash with aromatic residues in the catalytic center of the enzyme (e.g., Y65). Therefore, we were surprised that pyrroloC and tC were efficient substrates for UCK2 due to their large polycyclic structures. Since we had previously studied only C5-modified uridine nucleosides, we compared our results with pyrroloC and tC against two cytidine analogues containing different size substitutions at the C5 position: 5-bromocytidine (5-BrCyd) and 5-iodocytidine (5-ICyd). As expected, UCK2 activity on these substrates was inversely related to the size of the C5 substituent. Surprisingly, pyrroloC and tC were both more efficient UCK2 substrates than 5-BrCyd (Figure 3e, Supporting Information Figure 11 and Supporting Information Table 6), despite their multicyclic structure. We hypothesize that the rigidity of the pyrroloC and tC structures presents less steric bulk in proximity to UCK2 Y65, and indeed docking studies show that both nucleosides are well accommodated in the UCK2 active site (Figure 3f and Supporting Information Figure 12). In addition, the extended π -systems of pyrroloC and tC could engage in productive stacking or van der Waals interactions with aromatic residues in the UCK2 active site, such as Phe83 (Figure 3f).

Live-Cell RNA Imaging. Efficient cellular RNA labeling with tC and pyrroloC upon UCK2 expression led us to pursue this system for imaging real-time RNA dynamics in living cells. Toward this goal, we treated UCK2-expressing HeLa cells with pyrroloC or tC and used confocal fluorescence microscopy to

detect labeled RNA. First, we explored compatibility with different excitation sources and filter sets. For confocal imaging, 405 nm excitation combined with a DAPI emission filter gives similar signal intensity for both pyrroloC and tC; however, tC can also be imaged using 405 nm excitation combined with a GFP emission filter (535 \pm 20 nm) due to its longer wavelength emissions, and indeed, this combination gives better signal and allowed us to reduce exposure time in half (Supporting Information Figure 13a). Therefore, we decided to use the tC/UCK2 pair for confocal imaging with 405 nm excitation combined with the GFP emission filter. First, we evaluated the cytotoxicity of tC and pyrroloC (Supporting Information Figure 14), allowing selection of a labeling concentration that balances cellular toxicity with incorporation efficiency. Next, we performed RNA labeling with different serum concentrations and in the presence of the RNA synthesis inhibitor ActD. We treated cells with 200 μ M tC and monitored fluorescence after 6 h. We observed tC fluorescence in the cytoplasm and nucleus with the enhanced signal at the nucleolus, the major site of rRNA synthesis (Supporting Information Figure 13b), consistent with incorporation into RNA transcripts. Fluorescence was decreased substantially with ActD co-treatment (Figure 4a), indicating that the majority of signal originates from tC-containing RNA transcripts as opposed to fluorescent tC metabolites (nucleotides). In addition, we found a 59% increase in the fluorescence signal when tC treatment was performed in the presence of 10% fetal bovine serum as compared to reduced serum concentrations (Figure 4a,b), in line with reports that RNA transcription is upregulated with increased growth rate.²² Next, we investigated the kinetics of RNA labeling with tC. We observed cellular fluorescence at time points as early as 30 min (Figure 4c,d), indicating that tC RNA labeling can be used to report on dynamic cellular processes. The fluorescence signal increased over time and reached a plateau at 6 h (Figure 4c and Supporting Information Figure 13b).

Next, we used tC RNA labeling to investigate global RNA synthesis and turnover during oxidative stress. Oxidative stress induces a number of changes in cellular physiology concomitant with alterations in translational and transcriptional programs,^{23,24} but the impact of oxidation on bulk RNA dynamics is still poorly understood. To investigate the RNA dynamics during stress conditions, we performed metabolic labeling with tC nucleoside during sodium arsenite-induced oxidative stress and imaged cells at multiple time points after initiating feeding and stress. We observed a biphasic response during arsenite stress—tC fluorescence increased during the first hour of treatment but then steadily decreased from 1 to 4 h of continuous arsenite exposure (Figure 4e,f). In contrast, tC accumulation in RNA in unstressed cells continuously increases during the course of 4 h (Figure 4c,d). In addition, NaAsO₂-treated cells displayed changes in nucleolar RNA

signal, exhibiting larger numbers of nucleoli with reduced size and more regular spherical shape as compared to irregularly shaped nucleoli in unstressed cells (Figure 4e). Since NaAsO₂ exposure could affect both RNA synthesis and degradation, we next performed a pulse-chase labeling experiment in order to specifically investigate RNA turnover. Cells were fed tC for 4 h followed by a 30 min chase in tC-free medium in the presence or absence of NaAsO₂. The fluorescence signal from tC-labeled RNA was strongly reduced (55%) during chase in AsO₂-containing medium, whereas tC-labeled RNA levels were only 18% reduced in unstressed cells during the 30 min chase (Figure 4g,h). Taken together, our studies show that bulk RNA degradation rapidly increases in response to NaAsO₂ stress, but they do not support an acute effect of arsenite stress on RNA synthesis. In addition, we find altered nucleolar RNA localization, which suggests that oxidative stress affects rRNA synthesis and/or processing.

Interestingly, further analysis of RNA localization upon NaAsO₂ treatment indicated the formation of cytoplasmic RNA foci that arose as early as 1 h after stress induction (Figure 4e,i and Supporting Information Figure 15). These foci were only present when NaAsO₂ stress was applied during tC feeding and were absent from unstressed cells (Figure 4c) or cells where NaAsO₂ was applied during the chase (i.e. after tC treatment) (Figure 4g). Furthermore, we found that pyrroloC-treated cells subjected to NaAsO₂ during incorporation could form similar foci (Supporting Information Figure 16). To categorize the observed foci, we compared them against known cytoplasmic RNA-based structures specific to oxidative stress conditions. Stress granules are RNA-protein condensates containing translationally stalled mRNA- and RNA-binding proteins that form rapidly after arsenite stress.²⁵ We tested whether our foci colocalized with the characteristic stress-granule protein G3BP1 using live-cell imaging and expression of G3BP1-mCherry together with tC labeling and NaAsO₂ treatment. As expected, G3BP1-mCherry exhibited diffuse cytosolic staining during normal growth conditions and rapidly formed micron-sized foci in the cytosol upon NaAsO₂ stress (Supporting Information Figure 17), but these foci did not colocalize with the tC-labeled RNA foci (Figure 4i), although they were frequently found in close proximity. Next, we investigated co-localization with the P-body protein DCP1A.²⁶ While P-bodies are present constitutively, their number has been shown to increase upon NaAsO₂ stress.²⁷ We imaged DCP1A-mCherry together with tC-labeled RNA but did not observe co-localization between the NaAsO₂-dependent RNA foci and P-bodies (Figure 4i and Supporting Information Figure 17). Finally, we combined tC RNA live-cell imaging with expression of the RNA helicase DDX6²⁸ and found that tC RNA foci consistently co-localized with DDX6-mCherry upon NaAsO₂ stress (Figure 4i and Supporting Information Figure 17). Furthermore, to investigate the nature of the RNA in these foci, we tested their sensitivity to different small-molecule RNA polymerase inhibitors. Foci formation was unaffected by α -amanitin, an RNA polymerase II inhibitor, but abolished with ActD treatment at concentrations specific for RNA polymerase I inhibition (Figure 4j and Supporting Information Figure 15). Taken together, our results show that a subset of RNA transcripts generated during arsenite stress accumulate in cytoplasmic foci together with DDX6. These foci are distinct from canonical stress granules and P-bodies and likely contain rRNA.

DISCUSSION

In this manuscript, we develop a strategy for whole transcriptome RNA imaging in living cells. We show through confocal fluorescence microscopy and nucleoside LC-QQQ-MS that overexpression of UCK2 enables metabolic RNA labeling and direct fluorescence imaging with fluorescent ribonucleoside cytidine analogues tC and pyrroloC. Compared to prior approaches that typically rely upon metabolic labeling with azide- or alkyne-modified nucleosides followed by bio-orthogonal conjugation with a suitable reactive fluorophore, our strategy is operationally simpler, compatible with live-cell imaging, and less prone to artifacts, resulting from cellular fixation and/or permeabilization and washing conditions.

We apply tC RNA labeling and confocal imaging in order to study the dynamics of RNA synthesis and turnover during the oxidative stress response. Our results show a dramatic and rapid increase in RNA turnover during sodium arsenite treatment, with a ~50% reduction in bulk RNA transcript levels transcribed before stress induction after only 30 min. In contrast, RNA synthesis rates appear largely unchanged in this initial period but then decline after more prolonged exposure to sodium arsenite. These RNA-specific effects likely play an important role in reshaping gene expression programs during the integrated stress response,²³ both by downregulating the abundance of individual mRNA transcripts and by affecting rRNA levels and ribosome availability. In addition, we identified the formation of cytoplasmic arsenite-induced RNA granules that colocalize with the RNA helicase DDX6 but do not colocalize with the stress granule marker G3BP1 or the P-body protein DCP1A. Since these granules were only formed when tC RNA labeling was performed in the presence of NaAsO₂ and not during a NaAsO₂ chase, we propose that they contain RNA transcripts that were synthesized during stress conditions. While we cannot formally exclude the possibility that tC structure is related to the formation of these granules, their observation using pyrrolo C labeling, and their absence during normal conditions, supports the idea that these structures are not solely an outcome of artificial nucleoside incorporation. Furthermore, we find that granule formation is sensitive to the RNA Pol I inhibitor ActD but largely insensitive to the RNA Pol II inhibitor α -amanitin, suggesting that granules contain rRNA. Interestingly, a recent study demonstrated defects in 45S rRNA processing upon sodium arsenite exposure.²⁹ We speculate that the accumulation of rRNA in cytoplasmic granules distinct from stress granules and P-bodies may be related to the elimination of misprocessed forms generated during oxidative stress. The accumulation of DDX6 in these structures is intriguing as DDX6 has been implicated in P-body assembly, mRNA decay, and translational repression^{26,30} but to the best of our knowledge is not known to interact with rRNA. Further characterization of these granular structures will be necessary to understand their components and formulate hypothesis, relating to their physiological relevance.

Our work demonstrates that fluorescent nucleosides can be incorporated into RNA through metabolic labeling and used to track RNA metabolism and intracellular trafficking. The key to this technology is judicious selection of nucleoside structure and overexpression of the ribonucleoside kinase UCK2. In the cellular systems that we investigated, UCK2 levels appear to be limiting for the uptake of modified ribonucleosides. As levels of this kinase vary across different cell types and are known to be

overexpressed in cancers,³¹ uptake and incorporation of fluorescent cytidine analogues could be applied to facilitate cell-specific labeling for diagnostic purposes.

The bicyclic and tricyclic cytidine analogues explored herein likely represent a privileged scaffold for RNA metabolic labeling, and further investigation of this class of modified nucleosides together with UCK2 engineering should lead to the development of fluorescent nucleosides with enhanced and varied spectral properties, improved cellular tolerance, and context-dependent fluorescence. Esbjorner and Wilhelmsson recently investigated the biological properties of synthetic mRNA containing the related tC^o fluorescent nucleobase analogue³² and demonstrated that these synthetic transcripts can be translated in cells, underscoring their compatibility with cellular systems. While we observe cytotoxicity after extended metabolic labeling with tC or pyrroloC, comparable dose-limiting cytotoxicity has been seen for other metabolically compatible modified ribonucleosides such as 4-thiouridine (4-SU) and 5-ethynyluridine (5-EU).³³ Nevertheless, these findings indicate that our system is best suited for short pulse labeling applications (e.g., 1–2 h treatments) as these will have minimal impact on cellular physiology. Furthermore, the development of brighter tC and pyrroloC analogues (allowing lower treatment concentrations) should help mitigate this limitation. While further work is needed to understand the full biological impact of ring-extended cytidine analogues on RNA-associated processes, the structures reported in this work and related chemotypes are a promising starting point for further fluorescent nucleoside development. Beyond tracking localization and metabolism, analogous approaches could be utilized to incorporate diversely functionalized nucleoside analogues as biophysical probes to explore nucleic acid structures and protein–RNA interactions in their native context. Indeed, nucleic acid chemists have reported a variety of fluorescent nucleobases,¹³ but to the best of our knowledge, these structures have been primarily utilized in the context of oligonucleotides generated synthetically or by *in vitro* transcription. We envision that integrating nucleoside chemistry, protein engineering, and metabolic labeling should lead to unique opportunities for probing the dynamic behavior of RNA in its native biological context.

■ ASSOCIATED CONTENT

SI Supporting Information

The Supporting Information is available free of charge at <https://pubs.acs.org/doi/10.1021/jacs.2c04142>.

Experimental methods, compound synthesis and characterization, LC-QQQ-MS data, fluorescence microscopy data, and cell viability analysis (PDF)

■ AUTHOR INFORMATION

Corresponding Authors

Byron W. Purse – Department of Chemistry and Biochemistry and the Viral Information Institute, San Diego State University, San Diego, California 92182, United States; orcid.org/0000-0002-0052-6067; Email: bpurse@sdsu.edu

Ralph E. Kleiner – Department of Chemistry, Princeton University, Princeton, New Jersey 08544, United States; orcid.org/0000-0003-0508-9975; Email: rkleiner@princeton.edu

Authors

Danyang Wang – Department of Chemistry, Princeton University, Princeton, New Jersey 08544, United States; orcid.org/0000-0003-3678-0996

Ana Shalamberidze – Department of Chemistry and Biochemistry and the Viral Information Institute, San Diego State University, San Diego, California 92182, United States

A. Emilia Arguello – Department of Chemistry, Princeton University, Princeton, New Jersey 08544, United States

Complete contact information is available at:

<https://pubs.acs.org/10.1021/jacs.2c04142>

Notes

The authors declare no competing financial interest.

■ ACKNOWLEDGMENTS

We thank Gary Laevsky at the Princeton University Confocal Imaging Facility for assistance with live-cell fluorescence microscopy. We are grateful to David Sanders and Clifford Brangwynne for providing expression plasmids for G3BP1, DDX6, and DCPIA. R.E.K. acknowledges support from a National Science Foundation CAREER award (MCB-1942565), the National Institute of Health (R01 GM132189), and the Alfred P. Sloan Foundation. B.W.P. acknowledges the National Science Foundation (CHE-1800529 and CHE-2102642) for financial support. A.E.A. was supported by an Eli Lilly-Edward C. Taylor Fellowship in Chemistry.

■ REFERENCES

- (1) Braselmann, E.; Rathbun, C.; Richards, E. M.; Palmer, A. E. Illuminating RNA Biology: Tools for Imaging RNA in Live Mammalian Cells. *Cell Chem. Biol.* **2020**, *27*, 891–903.
- (2) Bertrand, E.; Chartrand, P.; Schaefer, M.; Shenoy, S. M.; Singer, R. H.; Long, R. M. Localization of ASH1 mRNA particles in living yeast. *Mol. Cell* **1998**, *2*, 437–445.
- (3) Paige, J. S.; Wu, K. Y.; Jaffrey, S. R. RNA mimics of green fluorescent protein. *Science* **2011**, *333*, 642–646.
- (4) Abudayyeh, O. O.; Gootenberg, J. S.; Essletzbichler, P.; Han, S.; Joung, J.; Belanto, J. J.; Verdine, V.; Cox, D. B. T.; Kellner, M. J.; Regev, A.; et al. RNA targeting with CRISPR-Cas13. *Nature* **2017**, *550*, 280–284.
- (5) Klöcker, N.; Weissenboeck, F. P.; Rentmeister, A. Covalent labeling of nucleic acids. *Chem. Soc. Rev.* **2020**, *49*, 8749–8773.
- (6) Kleiner, R. E. Interrogating the transcriptome with metabolically incorporated ribonucleosides. *Mol. Omics* **2021**, *17*, 833–841.
- (7) Qu, D.; Zhou, L.; Wang, W.; Wang, Z.; Wang, G.; Chi, W.; Zhang, B. 5-Ethynylcytidine as a new agent for detecting RNA synthesis in live cells by “click” chemistry. *Anal. Biochem.* **2013**, *434*, 128–135. Curanovic, D.; Cohen, M.; Singh, I.; Slagle, C. E.; Leslie, C.; Jaffrey, S. R. Global profiling of stimulus-induced polyadenylation in cells using a poly(A) trap. *Nat. Chem. Biol.* **2013**, *9*, 671–673. Grammel, M.; Hang, H.; Conrad, I. Chemical reporters for monitoring RNA synthesis and poly(A) tail dynamics. *ChemBioChem* **2012**, *13*, 1112–1115. Jao, C. Y.; Salic, A. Exploring RNA transcription and turnover *in vivo* by using click chemistry. *Proc. Natl. Acad. Sci. U. S. A.* **2008**, *105*, 15779–15784.
- (8) Wang, D.; Zhang, Y.; Kleiner, R. E. Cell- and Polymerase-Selective Metabolic Labeling of Cellular RNA with 2'-Azidocytidine. *J. Am. Chem. Soc.* **2020**, *142*, 14417–14421. Nainar, S.; Cuthbert, B. J.; Lim, N. M.; England, W. E.; Ke, K.; Sophal, K.; Quechol, R.; Mobley, D. L.; Goulding, C. W.; Spitale, R. C. An optimized chemical-genetic method for cell-specific metabolic labeling of RNA. *Nat. Methods* **2020**, *17*, 311–318.

- (9) Zhang, Y.; Kleiner, R. E. A Metabolic Engineering Approach to Incorporate Modified Pyrimidine Nucleosides into Cellular RNA. *J. Am. Chem. Soc.* **2019**, *141*, 3347–3351.
- (10) Nainar, S.; Beasley, S.; Fazio, M.; Kubota, M.; Dai, N.; Corrêa, I. R., Jr.; Spitale, R. C. Metabolic Incorporation of Azide Functionality into Cellular RNA. *ChemBioChem* **2016**, *17*, 2149–2152.
- (11) Kubota, M.; Nainar, S.; Parker, S. M.; England, W.; Furche, F.; Spitale, R. C. Expanding the Scope of RNA Metabolic Labeling with Vinyl Nucleosides and Inverse Electron-Demand Diels-Alder Chemistry. *ACS Chem. Biol.* **2019**, *14*, 1698–1707. Liu, H. S.; Ishizuka, T.; Kawaguchi, M.; Nishii, R.; Kataoka, H.; Xu, Y. A Nucleoside Derivative 5-Vinyluridine (VrU) for Imaging RNA in Cells and Animals. *Bioconjugate Chem.* **2019**, *30*, 2958–2966.
- (12) Rostovtsev, V. V.; Green, L. G.; Fokin, V. V.; Sharpless, K. B. A stepwise huisgen cycloaddition process: copper(I)-catalyzed regioselective "ligation" of azides and terminal alkynes. *Angew. Chem., Int. Ed. Engl.* **2002**, *41*, 2596–2599.
- (13) Xu, W.; Chan, K. M.; Kool, E. T. Fluorescent nucleobases as tools for studying DNA and RNA. *Nat. Chem.* **2017**, *9*, 1043–1055.
- (14) Berry, D. A.; Jung, K. Y.; Wise, D. S.; Sercel, A. D.; Pearson, W. H.; Mackie, H.; Randolph, J. B.; Somers, R. L. Pyrrolo-dC and pyrrolo-C: Fluorescent analogs of cytidine and 2'-deoxycytidine for the study of oligonucleotides. *Tetrahedron Lett.* **2004**, *45*, 2457–2461.
- (15) Preus, S.; Kilså, K.; Wilhelmsson, L. M.; Albinsson, B. Photophysical and structural properties of the fluorescent nucleobase analogues of the tricyclic cytosine (tC) family. *Phys. Chem. Chem. Phys.* **2010**, *12*, 8881–8892.
- (16) Sinkeldam, R. W.; Greco, N. J.; Tor, Y. Fluorescent analogs of biomolecular building blocks: design, properties, and applications. *Chem. Rev.* **2010**, *110*, 2579–2619. Liu, C.; Martin, C. T. Fluorescence characterization of the transcription bubble in elongation complexes of T7 RNA polymerase. *J. Mol. Biol.* **2001**, *308*, 465–475.
- (17) Seela, F.; Sirivolu, V. R. Pyrrolo-dC oligonucleotides bearing alkynyl side chains with terminal triple bonds: synthesis, base pairing and fluorescent dye conjugates prepared by the azide-alkyne "click" reaction. *Org. Biomol. Chem.* **2008**, *6*, 1674–1687.
- (18) Stengel, G.; Urban, M.; Purse, B. W.; Kuchta, R. D. Incorporation of the fluorescent ribonucleotide analogue tCTP by T7 RNA polymerase. *Anal. Chem.* **2010**, *82*, 1082–1089.
- (19) Engman, K. C.; Sandin, P.; Osborne, S.; Brown, T.; Billeter, M.; Lincoln, P.; Norden, B.; Albinsson, B.; Wilhelmsson, L. M. DNA adopts normal B-form upon incorporation of highly fluorescent DNA base analogue tC: NMR structure and UV-Vis spectroscopy characterization. *Nucleic Acids Res.* **2004**, *32*, 5087–5095. Lin, K.-Y.; Jones, R. J.; Matteucci, P. Tricyclic 2'-Deoxycytidine Analogs: Syntheses and Incorporation into Oligodeoxynucleotides Which Have Enhanced Binding to Complementary RNA. *J. Am. Chem. Soc.* **1995**, *117*, 3873–3874.
- (20) Teppang, K. L.; Lee, R. W.; Burns, D. D.; Turner, M. B.; Lokensgard, M. E.; Cooksy, A. L.; Purse, B. W. Electronic Modifications of Fluorescent Cytidine Analogues Control Photo-physics and Fluorescent Responses to Base Stacking and Pairing. *Chemistry* **2019**, *25*, 1249–1259.
- (21) Burns, D. D.; Teppang, K. L.; Lee, R. W.; Lokensgard, M. E.; Purse, B. W. Fluorescence Turn-On Sensing of DNA Duplex Formation by a Tricyclic Cytidine Analogue. *J. Am. Chem. Soc.* **2017**, *139*, 1372–1375. Rodgers, B. J.; Elsharif, N. A.; Vashisht, N.; Mingus, M. M.; Mulvahill, M. A.; Stengel, G.; Kuchta, R. D.; Purse, B. W. Functionalized tricyclic cytosine analogues provide nucleoside fluorophores with improved photophysical properties and a range of solvent sensitivities. *Chemistry* **2014**, *20*, 2010–2015.
- (22) Molina, N.; Suter, D. M.; Cannavo, R.; Zoller, B.; Gotic, I.; Naef, F. Stimulus-induced modulation of transcriptional bursting in a single mammalian gene. *Proc. Natl. Acad. Sci. U. S. A.* **2013**, *110*, 20563–20568.
- (23) Himanen, S. V.; Sistonen, L. New insights into transcriptional reprogramming during cellular stress. *J. Cell Sci.* **2019**, *132*, jcs238402.
- (24) Gerashchenko, M. V.; Lobanov, A. V.; Gladyshev, V. N. Genome-wide ribosome profiling reveals complex translational regulation in response to oxidative stress. *Proc. Natl. Acad. Sci. U. S. A.* **2012**, *109*, 17394–17399.
- (25) Protter, D. S. W.; Parker, R. Principles and Properties of Stress Granules. *Trends Cell Biol.* **2016**, *26*, 668–679.
- (26) Luo, Y.; Na, Z.; Slavoff, S. A. P-Bodies: Composition, Properties, and Functions. *Biochemistry* **2018**, *57*, 2424–2431.
- (27) Kedersha, N.; Stoecklin, G.; Ayodele, M.; Yacono, P.; Lykke-Andersen, J.; Fritzler, M. J.; Scheuner, D.; Kaufman, R. J.; Golan, D. E.; Anderson, P. Stress granules and processing bodies are dynamically linked sites of mRNP remodeling. *J. Cell Biol.* **2005**, *169*, 871–884.
- (28) Weston, A.; Sommerville, J. Xp54 and related (DDX6-like) RNA helicases: roles in messenger RNP assembly, translation regulation and RNA degradation. *Nucleic Acids Res.* **2006**, *34*, 3082–3094.
- (29) Szafarski, W.; Leśniczak-Staszak, M.; Sowiński, M.; Ojha, S.; Aulas, A.; Dave, D.; Malla, S.; Anderson, P.; Ivanov, P.; Lyons, S. M. Early rRNA processing is a stress-dependent regulatory event whose inhibition maintains nucleolar integrity. *Nucleic Acids Res.* **2022**, *50*, 1033–1051.
- (30) Coller, J.; Parker, R. General translational repression by activators of mRNA decapping. *Cell* **2005**, *122*, 875–886. Minshall, N.; Kress, M.; Weil, J.; Standart, R. Role of p54 RNA helicase activity and its C-terminal domain in translational repression, P-body localization and assembly. *Mol. Biol. Cell* **2009**, *20*, 2464–2472. Decker, C. J.; Parker, R. P-bodies and stress granules: possible roles in the control of translation and mRNA degradation. *Cold Spring Harbor Perspect. Biol.* **2012**, *4*, a012286.
- (31) Wu, Y.; Jamal, M.; Xie, T.; Sun, J.; Song, T.; Yin, Q.; Li, J.; Pan, S.; Zeng, X.; Xie, S.; et al. Uridine-cytidine kinase 2 (UCK2): A potential diagnostic and prognostic biomarker for lung cancer. *Cancer Sci.* **2019**, *110*, 2734–2747.
- (32) Baladi, T.; Nilsson, J. R.; Gallud, A.; Celauro, E.; Gasse, C.; Levi-Acobas, F.; Sarac, I.; Hollenstein, M. R.; Dahlén, A.; Esbjörner, E. K.; et al. Stealth Fluorescence Labeling for Live Microscopy Imaging of mRNA Delivery. *J. Am. Chem. Soc.* **2021**, *143*, 5413–5424.
- (33) Tani, H.; Mizutani, R.; Salam, K. A.; Tano, K.; Ijiri, K.; Wakamatsu, A.; Isogai, T.; Suzuki, Y.; Akimitsu, N. Genome-wide determination of RNA stability reveals hundreds of short-lived noncoding transcripts in mammals. *Genome Res.* **2012**, *22*, 947–956.